Check for updates

Achieving adjustable elasticity with non-affine to affine transition

Xiangying Shen [1,2,3], Chenchao Fang [1,3], Zhipeng Jin [1,3], Hua Tong [4,5], Shixiang Tang[1], Hongchuan Shen[1], Ning Xu [6], Jack Hau Yung Lo [1✉], Xinliang Xu [2,7 ✉] and Lei Xu [1,3 ✉]

For various engineering and industrial applications it is desirable to realize mechanical systems with broadly adjustable elasticity to respond flexibly to the external environment. Here we discover a topology-correlated transition between affine and non-affine regimes in elasticity in both two- and three-dimensional packing-derived networks. Based on this transition, we numerically design and experimentally realize multifunctional systems with adjustable elasticity. Within one system, we achieve solid-like affine response, liquid-like non-affine response and a continuous tunability in between. Moreover, the system also exhibits a broadly tunable Poisson's ratio from positive to negative values, which is of practical interest for energy absorption and for fracture-resistant materials. Our study reveals a fundamental connection between elasticity and network topology, and demonstrates its practical potential for designing mechanical systems and metamaterials.

Metamaterials[1] are artificial materials with unusual properties difficult to find in nature. These properties originate mainly from their structures rather than from their compositions. In particular, mechanical metamaterials[2–11] are specially designed structures with unusual elastic responses, such as negative Poisson's ratio[3,4], negative compressibility[5], non-reciprocity[6], topological boundary modes[7] and ultrahigh stiffness[8]. Adjustable mechanical metamaterials with elasticities that can be self-adjusted[9–11] are of enormous interest for industrial and engineering applications. Such materials have mostly been achieved by regular combination of identical units. However, disordered jamming structures, which are physically well defined and allow rigorous mathematical analysis, were recently discovered as another promising approach[3,4,10]. In this study, we realize multifunctional elastic systems inspired by disordered jamming structures.

Jamming is a special state in material packing that occurs in a wide range of situations, such as the jamming of particles, emulsions and foams [12–16], traffic jams, tumour progression[17] and even in embryonic morphogenesis[18]. At the jamming transition, rigidity arises and the system changes from fluid-like to solid-like[19–21]. However, a marginally jammed solid near the jamming transition differs substantially from a typical solid: for a typical solid, different moduli such as the shear modulus (G) and the bulk modulus (K) are closely related with a roughly constant ratio, whereas for a marginally jammed solid the shear modulus approaches zero but the bulk modulus remains finite, making their ratios diverge[22–24]. This $G \ll K$ behaviour is similar to that of a liquid, which is easy to shear but difficult to compress. Extensive studies[12–16,19–38] have demonstrated that the unique elastic properties near jamming come from the non-affine response, which indicates to what extent the internal strain is independent from the external load. The non-affine properties also enable amazing designs of disordered metamaterials based on jamming[3,4,10]. However, an important issue remains open: can such a non-affine system turn into an affine one, and realize both affine and non-affine elasticities within one single system? The short answer is yes.

We first illustrate this issue in two dimensions. The network is derived from a two-dimensional (2D) packing system with N particles, as shown in Fig. 1a: to prevent crystallization, the particles have two sizes with a size ratio of 1:1.4 and a number ratio of 1:1. The total number of contacts between particles is N_C and the contact interaction is harmonic with identical spring constant k. Based on this packing system, we construct a network with N nodes corresponding to N particles, and N_C bonds (that is, springs) corresponding to N_C contacts (Supplementary Information, section I). As illustrated in the upper part of Fig. 1a, we can vary the contact number by increasing the sizes of all the particles. As a result, more particles previously not in contact can touch each other, which corresponds to adding more bonds to the network, as illustrated in the lower part of Fig. 1a. During the particle inflation process, we keep all particle or node positions fixed and identical to the jamming point configuration, which makes the experimental operations simple and practical as demonstrated later.

Such a network satisfies the modified Maxwell isostatic theorem[39]:

$$dN - N_C = f(d) + N_0 - N_S \qquad (1)$$

where d is the dimension, $f(d) = d(d+1)/2$, N_0 is the number of floppy modes and N_S is the number of self-stress-states[40,41]. The coordination number, $z = 2N_C/N$, gives the average number of bonds per node. At the jamming point $N_0 = N_S$ and we obtain the isostatic condition: $z_C = 2N_C/N = 2d - 2f(d)/N \approx 2d$ for large enough N.

Above the jamming point (that is, $z > z_C$) the system changes from fluid-like to solid-like. However, a marginally jammed solid differs substantially from a typical solid. The underlying reason is the affine versus non-affine elastic response. The affine response comes from a linear correlation between the internal displacement

[1]Department of Physics, The Chinese University of Hong Kong, Hong Kong, China. [2]The Beijing Computational Science Research Center, Beijing, China. [3]Shenzhen Research Institute, The Chinese University of Hong Kong, Shenzhen, China. [4]School of Physics and Astronomy, Shanghai Jiao Tong University, Shanghai, China. [5]Department of Physics, University of Science and Technology of China, Hefei, China. [6]Hefei National Laboratory for Physical Sciences at the Microscale and Department of Physics, University of Science and Technology of China, Hefei, China. [7]Department of Physics, Beijing Normal University, Beijing, China. ✉e-mail: hylo@cuhk.edu.hk; xinliang@csrc.ac.cn; xuleixu@cuhk.edu.hk
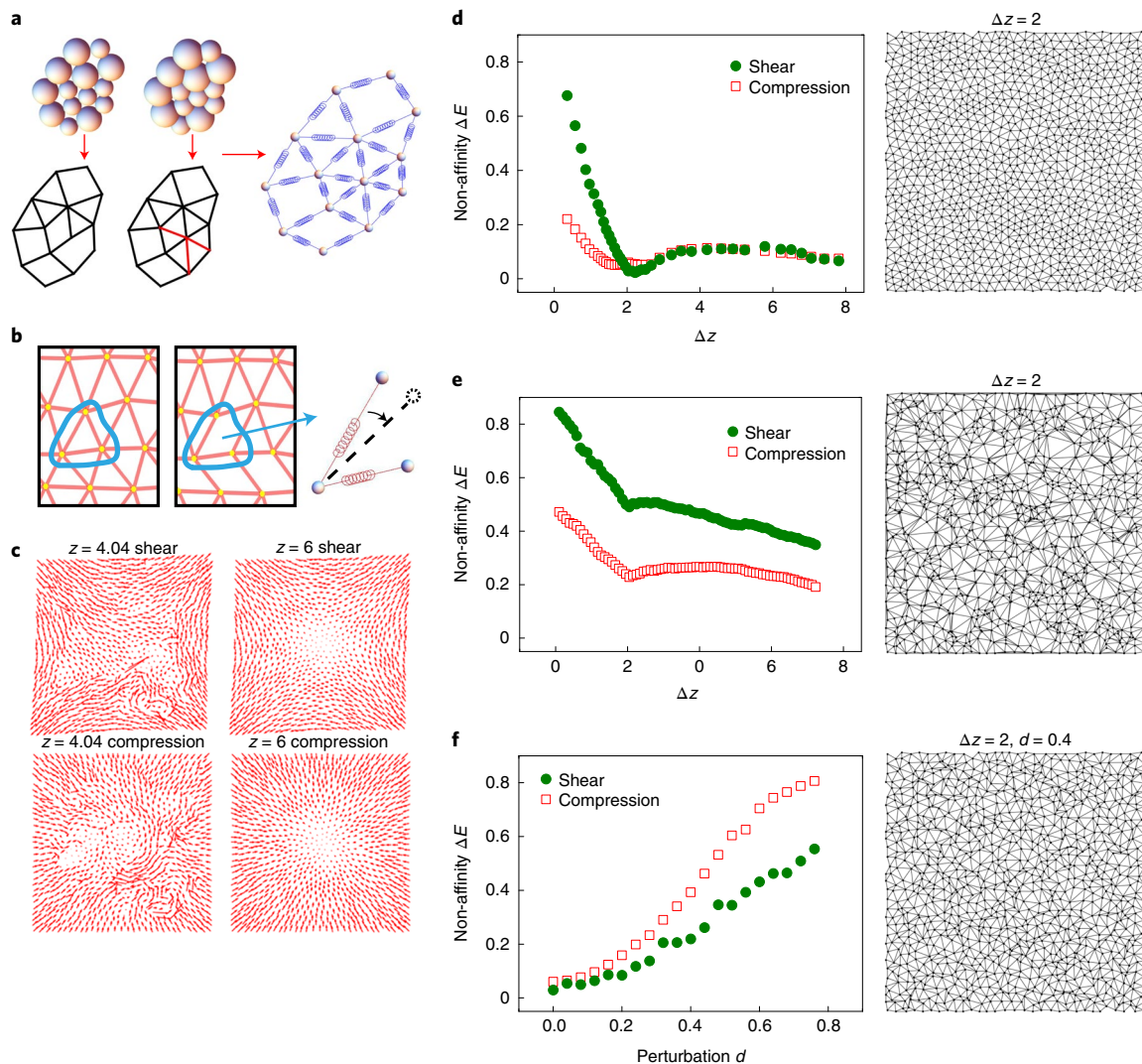
Fig. 1 | Non-affine to affine transition in packing-derived networks. a, Converting a particle-packing configuration into a spring network. Particles correspond to nodes and contacts correspond to bonds. We can vary the packing density by inflating the particles (upper), which increases the number of bonds in the network (lower). **b**, For the smallest patch with three nodes cut out of the system, three bonds are required to eliminate the floppy mode. If one bond is missing, one floppy mode will be created by free rotation. **c**, Displacement field before ($z=4.04$) and at ($z=6$) the non-affine to affine transition under shear and compression stress. The field is random before the transition and becomes linear at the transition. **d**, The non-affinity ΔE approaches zero at $\Delta z = z - z_c = 2$, indicating an almost ideal affine transition in our packing-derived network, the configuration of which is shown in the right-hand panel. **e**, ΔE never approaches zero in a random network, indicating its non-affine nature. Similar to **d**, a universal kink appears at $\Delta z = 2$, which separates two distinct elastic regimes. The right-hand panel shows the random network configuration. **f**, As every node position is perturbed from jamming configuration by larger and larger displacement d, the non-affinity ΔE at the kink $\Delta z = 2$ rises sharply, confirming that the affine transition uniquely occurs at the jamming point configuration, $d=0$. The right-hand panel shows the configuration at $d=0.4$ ($d=1$ is equivalent to the diameter of a small particle, which is close to an average bond length).

field and the external strain at the boundary, which typically appears in ordered or homogeneous structures. In disordered systems, however, their non-regular structures can disturb and destroy this linear correlation, and produce non-affine response. In general, ordered or homogeneous systems are typically affine, whereas disordered or inhomogeneous systems are non-affine. However, in this study we realize both affine and non-affine elasticities within a single disordered jamming network.

To realize the affine elasticity in a jamming system, we minimize the non-affinity or the characteristic length l^*, which is the typical size of a patch cut out from the system to create a floppy mode[28–30,40] (Supplementary Information, section IV). According to equation (1), l^* reaches a minimum when the system reaches

complete triangulation, as shown in Fig. 1b (Methods). Moreover, the 2D topologically invariant Euler characteristic further gives $z = 2N_C/N = 6 - 12/N \approx 6$ at this complete triangulation (Methods). Therefore, we identify a critical coordination number, $z_{aff} = 6$, at which the entire system reaches complete triangulation and the affine property reaches a maximum.

For direct visualization, we plot the internal displacement fields under external strain for $z<6$ and $z_{aff}=6$ in Fig. 1c. For $z<6$ the internal fields look rather random, while at $z_{aff}=6$ a linear correlation appears. Despite the underlying disordered structure, the system at $z_{aff}=6$ exhibits displacement fields almost identical to regular systems, confirming its affine nature (see Supplementary Information, section II for comparison with high-packing-density systems).

Above $z_{aff} = 6$, cross or intersecting bonds start to emerge and the system is no longer a planar graph[42–44]: the topology changes and the Euler characteristic breaks down. The system also goes beyond the typical packing scenario, as packed particles can only touch nearby neighbours and never penetrate through them to form cross bonds. Therefore, this transition corresponds to a fundamental change in both topology and packing scenario. To reach the cross-bond regime, we first connect all nearest neighbours in the system to reach complete triangulation, and then connect the next-nearest neighbours with cross bonds.

We further show that the minimum non-affinity achieved at $z_{aff} = 6$ actually approaches zero and the transition is affine. To quantify non-affinity, we define a dimensionless energy difference between the ideal affine displacement field and the actual displacement field: $\Delta E = (E_{aff} - E)/E_{aff}$. Here E_{aff} is the elastic energy stored in the affine displacement field mandatorily imposed according to a certain external strain, and E is the energy stored in the real displacement field under the same external strain. For any non-affine system, the mandatorily imposed affine displacement field is not a force equilibrium state and requires more energy than the real displacement field. Thus ΔE is non-negative and only approaches zero as the system approaches affine elasticity. In Fig. 1d (left-hand panel) we plot ΔE versus $\Delta z = z - z_C$ ($z_C = 4$ for two dimensions) in our system. For both shear and compression, there is a transition at $\Delta z = 2$ or $z_{aff} = 6$: to its left ΔE drops rapidly towards zero, and to its right ΔE is locked around a small value of about 0.1. This transition thus enables either a substantial adjustment or a lock-in capability. Moreover, ΔE approaches zero at $z_{aff} = 6$, indicating a non-affine to affine transition. We show its configuration in Fig. 1d (right-hand panel).

For comparison, we also calculate ΔE in a completely random system in Fig. 1e. Once again we observe a kink at $\Delta z = 2$, which separates two distinct regimes and reveals a general feature that the topology change at $\Delta z = 2$ produces two elastic regimes. However, Fig. 1e also differs substantially from Fig. 1d: at $\Delta z = 2$, ΔE is far above zero and thus the kink is not an affine transition. In fact, this random system remains highly non-affine throughout the entire Δz range, which could be a general feature for common disordered systems.

Therefore, the special combination of particle positions at the jamming configuration and bond connections at $\Delta z = 2$ lead to a non-affine to affine transition. To verify this, we perturb our system in Fig. 1f: as each particle is randomly displaced from the jamming configuration by larger and larger distance d, the non-affinity ΔE at $\Delta z = 2$ rises rapidly from zero. This unambiguously shows that the affine transition correlates closely to the jamming configuration, and perturbations in general destroy this affine transition. The underlying reason is probably the high local uniformity of the jamming configuration, which is similar to ordered lattice structures but in sharp contrast to the random system (see right-hand panels of Fig. 1d–e). Thus the jamming configuration's locally uniform node positions coupled with triangulated bond connections produce affine elasticity, and realize this ordered structure's property in a disordered system (Supplementary Fig. 3).

Apparently, besides the jamming transition at $z_C = 4$, there is another non-affine to affine transition at $z_{aff} = 6$. Our simulations on bulk and shear moduli K and G can directly verify this transition, as shown in Fig. 2a: two renormalized moduli, K/K_{max} and G/G_{max}, are plotted as a function of Δz. Clearly, near $\Delta z = 0$, G approaches zero while K remains finite, making their ratio, K/G, diverge (that is, highly non-affine). However, for $\Delta z > 2$ or $z > 6$, the two curves merge together, indicating a constant ratio of $K/G = K_{max}/G_{max}$; that is, affine-like behaviour. The inset further shows that only in sufficiently large systems, $N > 500$, does z_{aff} stabilize at 6. Fig. 2b plots the actual ratio, K/G, versus Δz for an $N = 1{,}024$ system: for $\Delta z < 2$, $K/G \approx \Delta z^{-1/2}$, which is different from the result of $K/G \approx \Delta z^{-1}$

reported in previous studies[38,45] due to our different bond-addition protocol with fixed particle positions; while for $\Delta z \geq 2$, $K/G \equiv 2$ and the system is affine-like.

To elucidate affine and non-affine elasticities, we derive a universal expression for an arbitrary modulus, M, in both affine and highly non-affine situations (Supplementary Information, section V):

$$M \propto kz \int_0^\pi \cos^2\alpha \times P(\alpha)\,d\alpha \qquad (2)$$

where α is the angle between an arbitrary bond and its two nodes' relative displacement due to external load (see Fig. 2c), and $P(\alpha)$ is the probability distribution of α in the entire system[31]. We theoretically calculate K and G with equation (2) and compare the results with numerical simulations in Fig. 2d,e, and observe a good agreement. Therefore, $P(\alpha)$ in equation (2) fundamentally explains affine and non-affine behaviours. In the non-affine regime, $P(\alpha)$ varies differently in K and G (refs. [31,45]), making K/G vary with z. In the affine regime, however, $P(\alpha)$ is fixed and thus K/G remains unchanged.

Combining affine and non-affine behaviours, we design networks with both types of tunability: our design is well above the jamming point $z_C = 4$ and closer to $z_{aff} = 6$, typically at $z > 5$ to ensure enough locally triangulated regions. One specific design is illustrated in the left-hand panel of Fig. 3a with $z = 5.28$. Clearly this network contains two distinct local structures: the affine regions with complete triangulation (that is, $z = 6$ locally) and the non-affine regions close to the jamming point structure (that is, $z = 4$ locally). These two types of regions exhibit distinct local properties (Supplementary Fig. 6), which form the basis of realizing the two-way tunability.

The non-affine regime enables us to adjust the ratio, K/G, across a broad range. Because some bonds make more contributions to K and some are more important to G (ref. [10]), deleting or adding such bonds can substantially change one modulus while keeping the other one stable. We first reduce K substantially by deleting the bonds important to K, as shown by the first two panels of Fig. 3a. The effect is shown in Fig. 3b: as the most important bonds are continuously deleted, K drops dramatically while G is relatively stable. It even reaches the unusual situation of $K < G$, as shown in the upper inset. Correspondingly, their ratio K/G decreases substantially as shown in the lower inset. Because K/G typically correlates to the Poisson's ratio, ν, this also tunes ν from positive to negative, as shown in Fig. 3c and Supplementary Video 1. Therefore, our network realizes non-affine elasticity and achieves a broad tunability in both K/G and ν.

We then demonstrate the affine-like behaviour with a constant K/G in the same network, based on the configuration shown in the middle panel of Fig. 3a. Clearly this configuration contains many triangulated regions with $z = 6$ locally. According to our previous result, when the global structure reaches complete triangulation, the system becomes an affine solid and $K/G \equiv 2$ is fixed. We now show that the elasticity is also correlated to local structures[40] (Supplementary Information, section VI). When cross bonds are added to the locally triangulated regions, as indicated by the red bonds in Fig. 3a (right-hand panel), both K and G increase while their ratio, K/G, remains a constant, as shown in Fig. 3d. Correspondingly, ν remains unchanged, as shown in Fig. 3e and Supplementary Video 2. More interestingly, now K/G is not just fixed at 2 but can be locked at an arbitrary value, such as 0.5 in this example, which provides an extra dimension of tunability (Supplementary Information, section VII).

Similar to Fig. 3a, we can also reduce G while keeping K relatively stable by deleting the bonds important to G only, as shown in Fig. 3f. This procedure decreases G by two orders of magnitude while keeping K relatively stable, as shown in Fig. 3g. Due to increasing anisotropy, this operation does not change ν substantially (Fig. 3h and Supplementary Information, section VIII). Based on
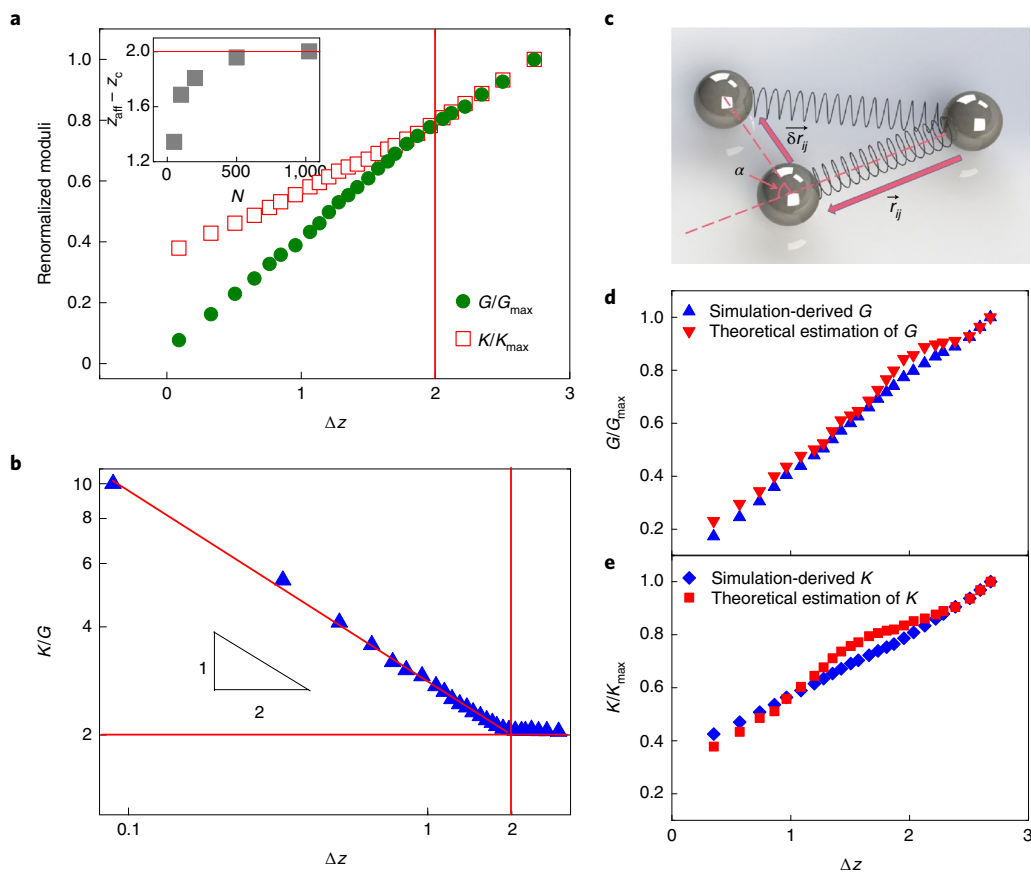
Fig. 2 | Understanding the variation of moduli at the single-particle level. a, The non-affine to affine transition at $\Delta z = 2$ in an $N = 1{,}024$ system. When $\Delta z < 2$, G/G_{max} and K/K_{max} vary differently; however, they collapse onto one curve for $\Delta z > 2$. The inset shows that the transition stabilizes at $\Delta z = 2$ for $N > 500$ systems. **b**, $K/G \approx \Delta z^{-1/2}$ before the transition while $K/G = 2$ after the transition. **c**, The schematics of the angle α between an arbitrary bond, $\vec{r}_{ij} = \vec{r}_j - \vec{r}_i$, and its two nodes' relative displacement under external stress, $\vec{\delta r}_{ij} = \vec{\delta r}_j - \vec{\delta r}_i$. **d**, Comparison between theory and simulation for renormalized shear modulus, G/G_{max}. **e**, Comparison between theory and simulation for renormalized bulk modulus, K/K_{max}. In both **d** and **e**, the agreement is reasonable, with the largest deviation being around 10–15%.

the configuration in Fig. 3f (middle panel), we again add cross bonds in the right-hand panel and confirm the affine function, as shown in Fig. 3i,j.

Combining affine and non-affine features, our network realizes three functions: (1) keeping K stable and substantially changing G; (2) keeping G stable and substantially changing K; and (3) keeping K/G stable and simultaneously changing K and G. All functions also apply to other pairs of moduli and thus achieve a broadly adjustable elasticity (Supplementary Information, section VII).

Next we realize this powerful system experimentally. The key issue is to eliminate the bending energy and realize pure harmonic interaction theoretically assumed. We use identical springs inside acrylic tubes as bonds and attach multiple bonds to one smooth rod that behaves as a node. All bonds can rotate freely around each node with negligible friction, which effectively eliminates the bending energy because all bonds prefer to rotate rather than bend. To avoid conflicts between cross bonds in the same plane, we design a multilayer system and place bonds at different heights, as shown in Fig. 4a–c. For simplicity, we design a small system with $N = 50$ nodes, and all bonds can be reversibly added or deleted (Supplementary Video 3).

Because the bulk modulus K cannot be measured easily, we measure the Young's modulus E and the shear modulus G (Methods). We first realize the non-affine property by substantially reducing E while changing G more gently. As shown in Fig. 4d, the coloured

bonds are continuously deleted, starting with the ones more important to E, which reduces E substantially while G changes more gently (see Fig. 4e). Correspondingly, E/G and ν change substantially in Fig. 4f. Similarly, we can reduce G substantially while keeping E relatively stable by deleting another set of bonds, as shown in Fig. 4g–i. These non-affine behaviours agree well with the simulations in Fig. 3.

We then realize the affine property in the same system. We first tune E and G to a desirable E/G, as shown by the black bonds in Fig. 4j. At this configuration, we then demonstrate the affine function by adding the cross bonds in triangulated regions, as shown by the coloured bonds. This varies both E and G simultaneously (see Fig. 4k), while keeping E/G and ν constant (see Fig. 4l). Thus we realize an independent tuning on E, G, E/G and ν, and achieve affine and non-affine elasticity experimentally.

Furthermore, all our 2D results can be extended to three dimensions. Similar to complete triangulation in two dimensions, when the network is fully tetrahedralized in three dimensions, a non-affine to affine transition appears (Methods). Our simulation confirms this transition at $z_{aff} = 12.8$ in Fig. 5b ($z_{aff} \neq 12$ due to poly-disperse particle size).

Above z_{aff}, cross bonds start to appear. Note that in three dimensions they go across a face, whereas in two dimensions they go across another bond, as shown in Fig. 5a. Similar to two dimensions, the 3D cross bonds also break a fundamental topology, the Euler–Poincaré
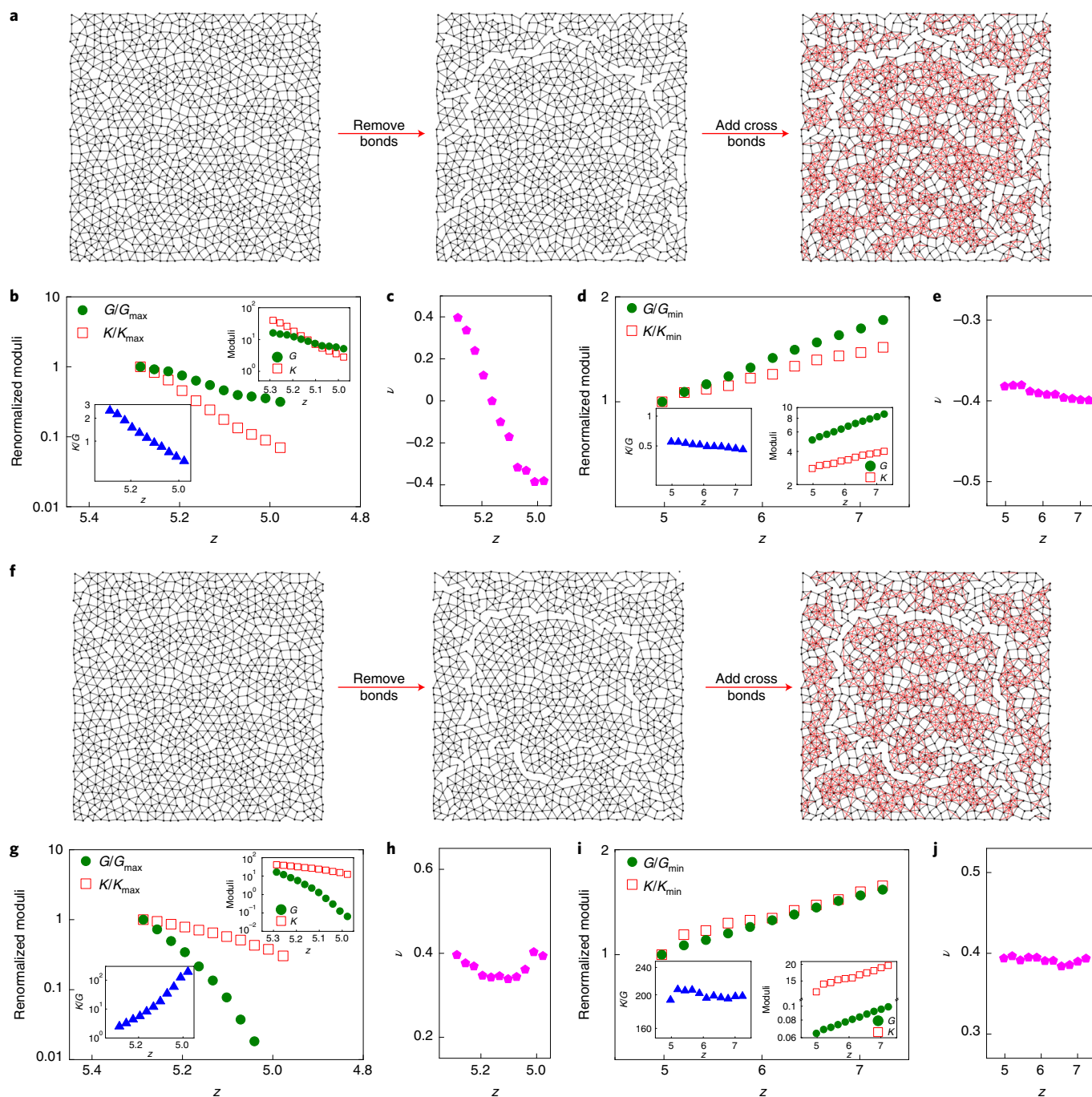
Fig. 3 | The numerical design of a network with both affine and non-affine tunability. a, The original network with $z = 5.28$ (left-hand panel); achieving non-affine tunability by removing the bonds important to K (middle panel); realizing affine tunability by adding the red cross bonds (right-hand panel). **b**, With the non-affine operation of bond removal, K reduces substantially while G changes more gently (note that the z axis decreases with this operation). Interestingly, K/G can decrease even below unity to reach the unusual situation of $K < G$ (insets). **c**, ν is also broadly tunable from positive to negative by this operation. **d**, With the affine operation of cross-bond addition, both K and G increase but K/G remains roughly constant (note that the z axis increases with this operation). **e**, ν also stays constant under this affine operation. **f**, Operations similar to **a** except that the bonds important to G are now removed and then the cross bonds are added. **g**, When the bonds important to G are removed, G reduces by two orders while K remains relatively stable. Correspondingly, K/G increases substantially. **h**, ν does not change much with bond removal. **i,j**, The affine operation of cross bond addition changes K and G simultaneously, while K/G (**i**) and ν (**j**) remain unchanged as expected.

characteristic[43], which is the 3D generalization of the Euler's characteristic in two dimensions (Supplementary Information, section X). Therefore, in both 2D and 3D packing-derived networks, a fundamental link between the non-affine to affine transition and the change in topology exists.

Analogous to two dimensions, adding cross bonds inside locally tetrahedralized regions can again lock the non-affinity. As shown in Fig. 5c, the non-affinity ΔE drops rapidly before z_{aff} and stabilizes around a small value after z_{aff}, confirming the non-affine and affine regimes. Moreover, we can tune ΔE, K/G or ν to a desirable value,
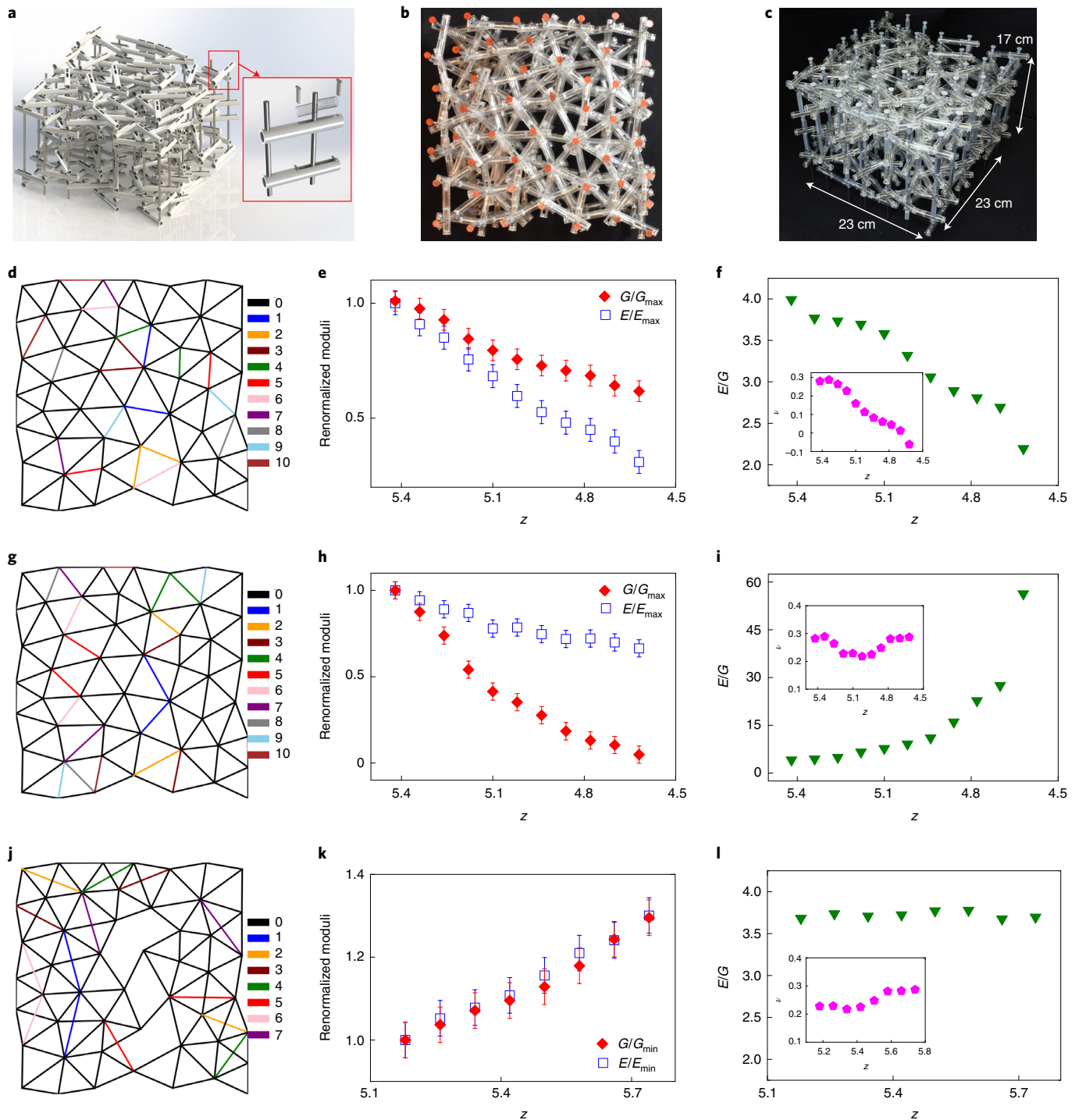
Fig. 4 | Experimental realization of affine and non-affine tunability. a, Schematics of our experimental system. The bonds are identical springs confined in acrylic tubes. The nodes are long rods for the bonds to hold on to. The system is designed as multilayered to avoid conflicts between crossing bonds, and as vertically symmetric to eliminate net torques. **b**, Top view image of the actual system with all nodes ($N = 50$) labelled in red. $z = 5.42$ in this system. **c**, Side view image of the actual system. **d**, Realizing the non-affine property by removing the coloured bonds which are critical to E in the order from 1 to 10, starting with the more important ones. **e**, The removal of bonds decreases E substantially but has much less effect on G. Note that both E and G are measured over two perpendicular directions and then averaged. **f**, The bond removal achieves broad adjustment on E/G and ν. **g**, Similar operation of bond removal for the ones critical to G only (shown in the order from 1 to 10). **h**, G reduces substantially while E decreases gently. **i**, The bond removal increases E/G substantially but ν does not change much. **j**, Realizing the affine property by adding the coloured cross bonds in the order from 1 to 7. **k**, With cross-bond addition both E and G increase at the same rate. **l**, E/G and ν stay unchanged, as expected for an affine system.

and then lock it by adding cross bonds, as shown by the triangle symbols and the inset. Therefore, all the affine and non-affine functions in two dimensions are realized in three dimensions.

For practical applications, realizing actual 3D metamaterials is essential. Using 3D printing, we achieve such metamaterials in Fig. 5d–f: the 5×5×5 node positions of these three networks are
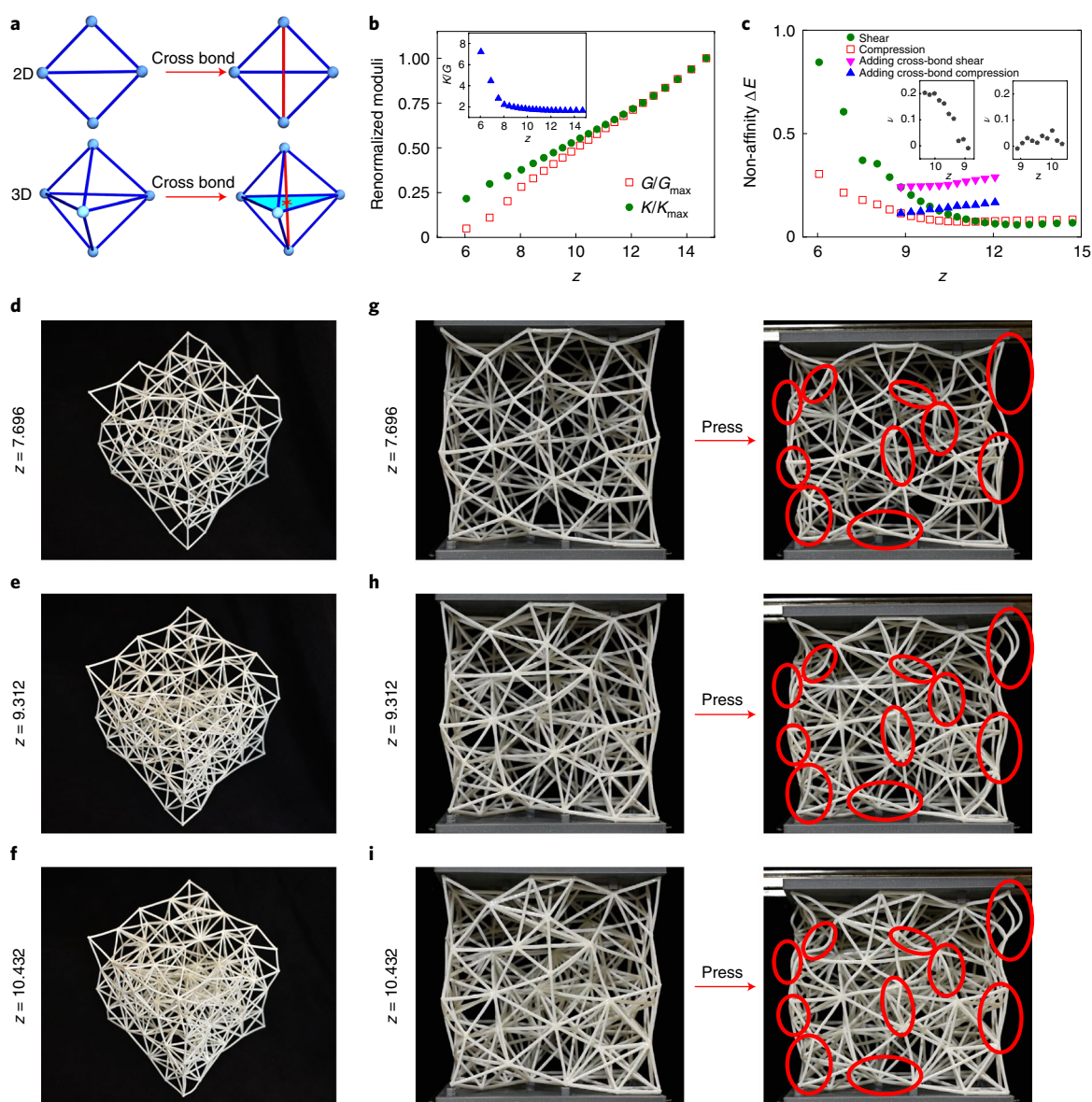
Fig. 5 | Extending the 2D results into three dimensions. a, Schematics showing the cross bond (denoted in red) in two and three dimensions. In two dimensions the cross bond goes across a bond and in three dimensions it goes across a face. **b**, G/G_{max} and K/K_{max} merge together above $z_{aff} = 12.8$ in a $32 \times 32 \times 32$ node packing-derived network, confirming the affine transition in three dimensions. Inset: K/G. **c**, The non-affinity ΔE under both shear and compression strain decreases with z and stabilizes in the affine regime of $z \geq 12.8$ (circles and squares). The triangles show the locking of non-affinity by adding cross bonds. Inset: tuning and locking of ν. **d–f**, side view of the 3D printed $5 \times 5 \times 5$ node networks at $z = 7.696$ (**d**), $z = 9.312$ (**e**) and $z = 10.432$ (**f**). These networks have identical node positions but different bond numbers or z. From the top to the middle panel, non-cross bonds are added which tunes the affinity K/G and ν. From the middle to the bottom panel, cross bonds are added which locks K/G and ν. **g–i**, Comparison of the internal strain fields of the three networks under an identical strain: $z = 7.696$ (**g**), $z = 9.312$ (**h**) and $z = 10.432$ (**i**). **g** and **h** exhibit different internal strain due to the tuning operation, while **h** and **i** exhibit similar internal strain due to the locking operation.

identical and from the same packing configuration, differing only in their bond number or z. From Fig. 5d to e, z increases from 7.696 to 9.312 by adding non-cross bonds, which tunes K/G and ν. From Fig. 5e to f, however, z increases from 9.312 to 10.432 by adding cross bonds, which locks K/G and ν while at the same time strengthening the system by increasing both K and G.

To verify their performance, we apply identical external strain to these three networks and compare their internal strain fields, which essentially determine the elastic responses such as non-affinity and Poisson's ratio. As illustrated in Fig. 5g–i, rows 1 and 2 exhibit substantial differences in internal strain, demonstrating distinct elastic responses due to our tuning operation; however, rows 2 and 3

show almost identical internal strains, verifying the same elastic responses due to our locking operation (see also Supplementary Videos 4 and 5). The forces generated by this strain are also measured as 7.86, 10.47 and 12.24 N, respectively, confirming the expected increase of system rigidity with respect to z. Note that our 3D printed bonds do exhibit bending force, which does not match the theoretical assumption perfectly. However, Fig. 5g–i still shows a good experimental outcome, demonstrating the robustness of our design, which paves the way for realizing actual metamaterials beyond ideal spring networks. We further note that all bonds can be 3D printed to be detachable to realize all functions in a single system (Supplementary Video 6). In addition, the size range of the

bonds and the overall system may vary by multiple orders to satisfy various practical requirements. The plasticity and failure behaviours can also withstand a broad range of external stress due to the heterogeneous structure, and avoid the sudden failure of ordered lattice systems, which are composed mostly of identical bonds that may fail simultaneously.

To conclude, we have discovered a non-affine to affine transition at the point of topology change. Based on this fundamental transition, we realize networks broadly tunable in K, G, K/G and ν, and achieve both affine and non-affine elasticities within one system. Moreover, such systems might be self-assembled by packing granular materials and control connections either chemically[46] or electrically with electromagnetic devices, which may greatly improve their practical applications. Our study reveals a fundamental connection between elasticity and topology, and provides a practical design principle for multifunctional mechanical metamaterials.

Online content

Any methods, additional references, Nature Research reporting summaries, source data, extended data, supplementary information, acknowledgements, peer review information; details of author contributions and competing interests; and statements of data and code availability are available at https://doi.org/10.1038/s41563-021-01046-8.

References

1. Kadic, M., Bückmann, T., Schittny, R. & Wegener, M. Metamaterials beyond electromagnetism. *Rep. Prog. Phys.* **76**, 126501 (2013).
2. Berger, J. B., Wadley, H. N. G. & McMeeking, R. M. Mechanical metamaterials at the theoretical limit of isotropic elastic stiffness. *Nature* **543**, 533–537 (2017).
3. Rocks, J. W. et al. Designing allostery-inspired response in mechanical networks. *Proc. Natl Acad. Sci. USA* **114**, 2520–2525 (2017).
4. Reid, D. R. et al. Auxetic metamaterials from disordered networks. *Proc. Natl Acad. Sci. USA* **115**, 1384–1390 (2018).
5. Nicolaou, Z. G. & Motter, A. E. Mechanical metamaterials with negative compressibility transitions. *Nat. Mater.* **11**, 608–613 (2012).
6. Coulais, C., Sounas, D. & Alù, A. Static non-reciprocity in mechanical metamaterials. *Nature* **542**, 461–464 (2017).
7. Kane, C. L. & Lubensky, T. C. Topological boundary modes in isostatic lattices. *Nat. Phys.* **10**, 39–45 (2014).
8. Zheng, X. et al. Ultralight, ultrastiff mechanical metamaterials. *Science* **344**, 1373–1377 (2014).
9. Coulais, C., Sabbadini, A., Vink, F. & van Hecke, M. Multi-step self-guided pathways for shape-changing metamaterials. *Nature* **561**, 512–515 (2018).
10. Goodrich, C. P., Liu, A. J. & Nagel, S. R. The principle of independent bond-level response: tuning by pruning to exploit disorder for global behavior. *Phys. Rev. Lett.* **114**, 225501 (2015).
11. Florijn, B., Coulais, C. & van Hecke, M. Programmable mechanical metamaterials. *Phys. Rev. Lett.* **113**, 175503 (2014).
12. Majmudar, T. S., Sperl, M., Luding, S. & Behringer, R. P. Jamming transition in granular systems. *Phys. Rev. Lett.* **98**, 058001 (2007).
13. Dauchot, O., Marty, G. & Biroli, G. Dynamical heterogeneity close to the jamming transition in a sheared granular material. *Phys. Rev. Lett.* **95**, 265701 (2005).
14. Keys, A. S., Abate, A. R., Glotzer, S. C., & Durian, D. J. Measurement of growing dynamical length scales and prediction of the jamming transition in a granular material. *Nat. Phys.* **4**, 260–264 (2007).
15. Alexander, S. Amorphous solids: their structure, lattice dynamics and elasticity. *Phys. Rep.* **296**, 65–236 (1998).
16. Silbert, L. E., Ertas, D., Grest, G. S., Halsey, T. C. & Levine, D. Geometry of frictionless and frictional sphere packings. *Phys. Rev. E* **65**, 031304 (2002).
17. Oswald, L., Grosser, S., Smith, D. M. & Kas, J. A. Jamming transitions in cancer. *J. Phys. D* **50**, 483001 (2017).
18. Mongera, A. et al. A fluid-to-solid jamming transition underlies vertebrate body axis elongation. *Nature* **561**, 401–405 (2018).
19. Liu, A. J. & Nagel, S. R. Jamming is not just cool any more. *Nature* **396**, 21–22 (1998).
20. Olsson, P. & Teitel, S. Critical scaling of shear viscosity at the jamming transition. *Phys. Rev. Lett.* **99**, 178001 (2007).
21. Head, D. A. Critical scaling and aging in cooling systems near the jamming transition. *Phys. Rev. Lett.* **102**, 138001 (2009).
22. Somfai, E., Roux, J. N., Snoeijer, J. H., Van Hecke, M. & Van Saarloos, W. Elastic wave propagation in confined granular systems. *Phys. Rev. E* **72**, 021301 (2005).
23. Makse, H. A., Gland, N., Johnson, D. L. & Schwartz, L. M. Why effective medium theory fails in granular materials. *Phys. Rev. Lett.* **83**, 5070 (1999).
24. Makse, H. A., Johnson, D. L. & Schwartz, L. M. Packing of compressible granular materials. *Phys. Rev. Lett.* **84**, 4160 (2000).
25. Zhang, Z. X. et al. Thermal vestige of the zero-temperature jamming transition. *Nature* **459**, 230–233 (2009).
26. Weitz, D. Packing in the spheres. *Science* **303**, 968–969 (2004).
27. Tkachenko, A. V. & Witten, T. A. Stress propagation through frictionless granular material. *Phys. Rev. E* **60**, 687 (1999).
28. Ellenbroek, W. G., van Hecke, M. & van Saarloos, W. Jammed frictionless disks: connecting local and global response. *Phys. Rev. E* **80**, 061307 (2009).
29. Wyart, M., Nagel, S. R. & Witten, T. A. Geometric origin of excess low-frequency vibrational modes in weakly connected amorphous solids. *Europhys. Lett.* **72**, 486 (2005).
30. Wyart, M., Silbert, L. E., Nagel, S. R. & Witten, T. A. Effects of compression on the vibrational modes of marginally jammed solids. *Phys. Rev. E* **72**, 051306 (2005).
31. Ellenbroek, W. G., Somfai, E., van Hecke, M. & Van Saarloos, W. Critical scaling in linear response of frictionless granular packings near jamming. *Phys. Rev. Lett.* **97**, 258001 (2006).
32. Donev, A., Torquato, S. & Stillinger, F. H. Pair correlation function characteristics of nearly jammed disordered and ordered hard-sphere packings. *Phys. Rev. E* **71**, 011105 (2005).
33. Silbert, L. E., Liu, A. J. & Nagel, S. R. Vibrations and diverging length scales near the unjamming transition. *Phys. Rev. Lett.* **95**, 098301 (2005).
34. Zhao, C., Tian, K. & Xu, N. New jamming scenario: from marginal jamming to deep jamming. *Phys. Rev. Lett.* **106**, 125503 (2011).
35. Mao, X., Xu, N. & Lubensky, T. C. Soft modes and elasticity of nearly isostatic lattices: randomness and dissipation. *Phys. Rev. Lett.* **104**, 085504 (2010).
36. Xu, N., Vitelli, V., Liu, A. J. & Nagel, S. R. Anharmonic and quasi-localized vibrations in jammed solids—modes for mechanical failure. *Europhys. Lett.* **90**, 56001 (2010).
37. Liu, A. J. & Nagel, S. R. The jamming transition and the marginally jammed solid. *Annu. Rev. Condens. Matter Phys.* **1**, 347–369 (2010).
38. van Hecke, M. Jamming of soft particles: geometry, mechanics, scaling and isostaticity. *J. Phys. Condens. Matter* **22**, 033101 (2010).
39. Calladine, C. R. Buckminster Fuller tensegrity structures and Clerk Maxwell rules for the construction of stiff frames. *Int. J. Solids Struct.* **14**, 161–172 (1978).
40. Wyart, M., Liang, H., Kabla, A. & Mahadevan, L. Elasticity of floppy and stiff random networks. *Phys. Rev. Lett.* **101**, 215501 (2008).
41. Lubensky, T. C., Kane, C. L., Mao, X., Souslov, A. & Sun, K. Phonons and elasticity in critically coordinated lattices. *Rep. Prog. Phys.* **78**, 073901 (2015).
42. Trudeau, R. J. *Introduction to Graph Theory* 64–116 (Dover, 1993).
43. Nakamura, N. *Geometry, Topology and Physics* 67–91 (Institute of Physics Publishing, 2008).
44. Giménez, O. & Noy, M. Asymptotic enumeration and limit laws of planar graphs. *J. Am. Math. Soc.* **22**, 309–329 (2009).
45. Ellenbroek, W. G., Zeravcic, Z., Van Saarloos, W. & Van Hecke, M. Non-affine response: jammed packings vs spring networks. *Europhys. Lett.* **87**, 34004 (2009).
46. Li, S. et al. Liquid-induced topological transformations of cellular microstructures. *Nature* **592**, 386–391 (2021).

Methods

Deriving the transition in two dimensions. The non-affinity will be minimized when l^* reaches a minimum, that is, no floppy mode can be created even in an arbitrary smallest patch. A smallest patch is formed by three nearby and non-collinear nodes and we apply the theorem of equation (1) to this three-node patch: no floppy mode means $N_0 = dN - N_C - f(d) + N_S = 0$. Plugging in $d = 2, N = 3, f(d) = 3, N_S = 0$ (no self-stress-state can exist in three non-collinear nodes), we get $N_C = 3$. This means three bonds are required for this three-node patch, that is, a triangle is needed for zero floppy mode, as shown in Fig. 1b (left-hand panel). If we eliminate one bond as shown in the right-hand panel, the three-node patch can now freely rotate without costing any energy, which creates one floppy mode. Therefore, to minimize l^* and non-affinity, three bonds are required for every three-node patch and the system achieves complete triangulation.

A completely triangulated configuration contains no intersecting or cross bonds and belongs to the planar graph, which obeys the topological invariant—the Euler characteristic: $N_f - N_C + N = 2$ (refs. [42,43]), where N_f is the number of faces enclosed by edges or bonds. For a triangulated large-N system whose boundary influence can be neglected, each face is surrounded by three bonds, and each bond is shared by two faces, and thus $3N_f = 2N_C$. Plugging $N_f = 2N_C/3$ into the Euler characteristic, we get: $N_C = 3N - 6$ and thus $z = 2N_C/N = 6 - 12/N \approx 6$. Thus at $z_{aff} = 6$ the system reaches the non-affine to affine transition.

Deriving the transition in three dimensions. The smallest patch in three dimensions is formed by four non-coplanar nodes and we apply the Maxwell isostatic theorem, $N_0 = dN - N_C - f(d) = 0$, to it. Plugging in $d = 3, N = 4, N_S = 0$ and $f(d) = 6$, we get $N_C = 6$. Thus the smallest patch without a floppy mode is a tetrahedron with four nodes and six bonds. Therefore, when the network is fully tetrahedralized, a non-affine to affine transition will appear.

Measuring E and G in the spring system. We first measure the stress by fixing one boundary of the system and moving the opposite boundary with 5% strain, in either parallel (G) or perpendicular (E) direction. We then divide the stress with the strain and obtain the modulus. Due to the boundary effect, these measurements still deviate by about 10% from the rigorous definition (Supplementary Information, section IX) but are good enough as experimental approximations.

Data availability

All the raw data of the figures presented in this manuscript can be obtained by accessing the Open Science Framework (https://doi.org/10.17605/OSF.IO/7EQ5Z) or directly visiting https://osf.io/7eq5z/ (ref. [47]).

Code availability

All custom computer code and algorithms used to generate the results reported in the paper are available upon request.

References

47. Shen, X. et al. *Achieving Adjustable Elasticity with Non-affine to Affine Transition* https://doi.org/10.17605/OSF.IO/7EQ5Z (OSF, 2021).

Author contributions

X.S. and C.F. contributed equally to this research. L.X. conceived the research. X.S., C.F., J.H.Y.L., X.X. and L.X. designed the research. X.S. performed most of the theoretical and numerical analysis. C.F. performed most of the experiments. Z.J., S.T., H.S., H.T. and N.X. helped in the experiments or the simulations. X.S., C.F. and L.X. prepared the manuscript. L.X. and X.X. supervised the research.

Competing interests

The authors declare no competing interests.

Additional information

Supplementary information The online version contains supplementary material available at https://doi.org/10.1038/s41563-021-01046-8.

Correspondence and requests for materials should be addressed to J.H.Y.L., X.X. or L.X.

Peer review information *Nature Materials* thanks Larry Howell, Yang Jiao, Zachary Nicolaou and the other, anonymous, reviewer(s) for their contribution to the peer review of this work.

Reprints and permissions information is available at www.nature.com/reprints.